
Article:
Espensen, CA, Kiilgaard, JF, Appelt, AL orcid.org/0000-0003-2792-9218 et al. (5 more authors) (2020) Dose-response and normal tissue complication probabilities after proton therapy for choroidal melanomas. Ophthalmology. ISSN 0161-6420

https://doi.org/10.1016/j.ophtha.2020.06.030

Dose-response and normal tissue complication probabilities after proton therapy for choroidal melanomas

Dose response after proton therapy for choroidal melanoma

Charlotte A Espensen[1,2], Jens F Kiilgaard[2,*], Ane L Appelt[3], Lotte S Fog[4,5], Joel Herault[6], Celia Maschi[7], Jean-Pierre Caujolle[7], Juliette Thariat[8,9,10]

Financial Support:

This work is supported by research grants from Synoptik-Foundation, the Danish Eye Research Foundation (Øjenfonden), the Danish Cancer Research Foundation (Dansk Kræftforsknings Fond), Aase and Ejnar Danielsens Foundation, and Arvid Nilssons Foundation. Ane Appelt is supported by Yorkshire Cancer Research Academic Fellowship funding (grant L389AA). The funding organizations had no role in the design or conduct of this research.

Conflicts of interest:

No conflicting relationship exists for any author.

This article contains additional online-only material. The following should appear online-only: Supplementary material (Appendix A-C).

[1] Department of Oncology, Section of Radiotherapy, Copenhagen University hospital, Rigshospitalet, Copenhagen, Denmark
[2] Department of Ophthalmology, Copenhagen University hospital, Rigshospitalet, Copenhagen, Denmark
[3] Leeds Institute of Medical Research at St James's, University of Leeds, and Leeds Cancer Centre, St James's University Hospital, Leeds, United Kingdom
[4] Department of Physical Sciences, The Peter MacCallum Cancer Centre, Melbourne, Australia
[5] Alfred Health Radiation Oncology, The Alfred, Melbourne, Victoria, Australia
[6] Department of Radiation Oncology, Centre Antoine-Lacassagne, Nice, France
[7] Department of Ophthalmology, Nice University Hospital, Nice, France
[8]Department of Radiation Oncology, Centre Francois Baclesse, Caen, France
[9] Laboratoire de Physique Corpusculaire IN2P3/ENSICAEN, Caen, France
[10] Unicaen – Normandy University, France
[*] Corresponding author

Abstract

Purpose

Normal tissue complication probability (NTCP) models could aid the understanding of dose-dependence of radiation-induced toxicities after eye-preserving radiotherapy of choroidal melanomas. We performed NTCP-modelling and established dose-response relationships for visual acuity deterioration and common late complications after treatments with proton therapy (PT).

Design

Retrospective study from single large referral centre.

Subjects

We considered patients diagnosed with choroidal melanoma and primarily treated with hypo-fractionated PT (52 Gy physical dose in 4 fractions). 1020 patients had complete visual acuity deterioration information, 991 patients had complete information on late complications.

Methods

Treatment details and dose-volume histograms (DVHs) for relevant anatomical structures and patient and tumour characteristics were available from a dedicated ocular database. Lasso variable selection was used to identify variables with the strongest impact on each endpoint, followed by multivariable Cox regressions and logistic regressions to analyse the relationship between dose, clinical characteristics and clinical outcomes. Dose-response relationships were estimated, adjusting for relevant clinical variables.

Main Outcome Measures

Dose-response relationship for visual acuity deterioration and late complications

Results

Dose metrics for several structures (i.e. optic disc, macula, retina, globe, lens, ciliary body) correlated with clinical outcome. The near-maximum dose to the macula (macula $D_{2\%}$) showed the strongest correlation with visual acuity deterioration. Retina $D_{20\%}$ was the only variable with clear impact on the risk of developing maculopathy; optic disc $D_{20\%}$ had the largest impact on optic neuropathy; cornea $D_{20\%}$ had the largest impact on neovascular glaucoma; ciliary body $D_{20\%}$ had the largest impact on ocular hypertension; the volume of the ciliary body receiving 26 Gy (ciliary body V_{26Gy}) was the only variable associated with the risk of cataract; and retina V_{52Gy} was associated with the risk of retinal detachment. Optic disc-tumour distance was the only variable associated with dry eye syndrome in the absence of DVH for the lachrymal gland.

Conclusions

Visual acuity deterioration and specific late complications demonstrated dependence on dose delivered to normal structures in the eye after PT for choroidal melanoma. Visual acuity deterioration depended on dose to a range of structures, while more specific complications were primarily related to dose metrics for specific structures.

Introduction

Eye-preserving proton therapy is commonly used to treat choroidal melanomas [1]. The ultimate objective of the treatment is to destroy the malignancy without producing complications on adjacent healthy tissues, thereby preserving long term function. Nonetheless, some structures may be exposed to large doses during treatment, and radiation-induced visual deterioration and toxicities are common side-effects [2]. Normal tissue complication probability (NTCP) models for most complications have not yet been established for hypo-fractionated proton therapy and the relevance of damage to the various ocular structures has not been fully examined. To rectify this, we examined data from a large cohort of patients treated at a dedicated proton therapy facility, with long follow-up. We conducted dose-response modelling to examine the relationships between dose delivered to healthy tissue and the occurrence of visual acuity deterioration and various radiation-induced toxicities.

Materials and methods

Patients

This retrospective study included patients treated for choroidal melanomas between 1991 and 2015 at a dedicated proton centre. Patients and tumour characteristics as well as treatment details were prospectively registered in an ocular database.

Post-treatment visits, with tumour assessment by an onco-ophthalmologist and liver ultrasound, were performed every sixth months the first two years and annually subsequently. Patients were followed until at least 5 years after treatment if possible. At each visit, the Snellen' scale was used to evaluate the best corrected visual acuity, and fundus photography and/or fluorescein angiography were used to examine the fundus. Furthermore, tumour thickness and diameter were measured at each visit using ultrasound. Complications were recorded prospectively at each clinical visit.

Information on recurrence, secondary enucleation, and side-effects were collected [3]. For the purpose of this study, patient and tumour characteristics as well as treatment and outcome data were retrospectively extracted from the database; with patients with missing information on general characteristics and/or outcomes excluded. The study was retrospective and received a waiver of informed consent approved by the Ethics Committee of the French Society of Ophthalmology (IRB 00008855 Société Française d'Ophtalmologie IRB#1) and the research adhered to the tenets of the Declaration of Helsinki.

Treatment and planning

Protons with energy of 65 MeV were produced by a fixed-frequency cyclotron. The construction and the physics of the aperture and beam have previously been described [4–6]. EyePlan (version 3.06) was used as treatment planning system (TPS). Experienced dosimetrists created each plan in close cooperation with radiation oncologists, choosing the modulator, the collimator shape and angles for eye orientation. Each tumour received a physical tumour dose of 52 Gy in 4 fractions of 13 Gy, delivered on 4 consecutive days [3]. This planning and treatment have previously been described in detail [7]. Figure 1 illustrates the main steps of the treatment planning. Dose-volume histograms for each of the relevant anatomical structures were extracted from the TPS. Physical doses were used for all analyses and no correction from fraction size effects was thus employed. Dose volume histograms (DVHs) or dose surface histograms (DSHs) were extracted for each normal tissue structure. A range of dose metrics were calculated to represent the entire DVH/DSH while still limiting the number of variables in the analysis and avoiding excessive collinearity between variables. These included the volume or the surface treated to a specific (discretised) dose level x (Vx/Sx), or the dose delivered to a specific volume or surface y (Dy) (V/S_{52Gy}, V/S_{42Gy}, V/S_{26Gy}, V/S_{10Gy}, V/S_{5Gy}, $D_{98\%}$, $D_{50\%}$, $D_{20\%}$ and $D_{2\%}$). We prioritised metrics representing the

'extremes' of the dose distribution as well 'mid-range' of the DVHs. Details on the treatments and planning are described further in Appendix A.

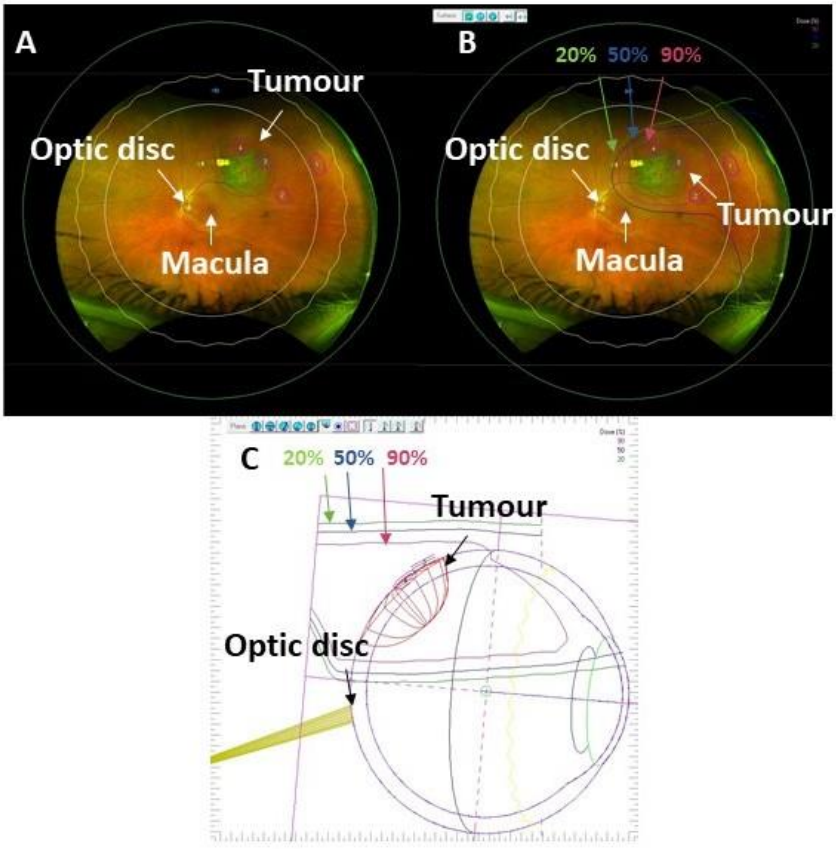

Figure 1: The steps in 3D image-guided treatment planning using EyePlan. A) Tumour contouring in the exact location on pre-treatment fundus photography. B) Three levels of isodoses. Dose levels 90% (purple), 50% (dark blue), and 20% (green) are used for illustrative purposes. C) 3D illustration of the treatment plan, the tumour, optic disc, and the isodose levels.

Definition of toxicity and complications

Visual acuity deterioration

Visual acuity was measured using the Snellen scale. For analysis purposes it was converted into the logarithm of Minimum Angle of Resolution (logMAR) scale [8,9]; this has been used throughout the analyses. Longitudinal measures were not available for visual acuity, and the analysis was thus entirely based on the measure from last follow-up. We defined visual acuity deterioration of ≥ 0.3 logMAR compared to the baseline measure.

Posterior complications

Maculopathy: Radiation-induced maculopathy was diagnosed based on visual acuity deterioration and the presence of micro-aneurysms, ischemia and/or oedema in the entire macular region, assessed by ophthalmoscopy or preferable visualized from fundus photography and optical coherence tomography (OCT).

Optic neuropathy: Ophthalmoscopy was used to diagnose the condition. An oedematous and/or atrophic optic disc in combination with a considerable decrease in visual acuity were the most common observations in the diagnosis of radiation-induced optic neuropathy (RION). Additionally, an undelimited and pale disc was used in the diagnosis.

Ocular hypertension: Ocular hypertension was defined as intraocular pressure (IOP) higher than 21 mmHg at multiple measurements without signs of visual field defects or cupping of the disc.

Neovascular glaucoma: In cases of elevated IOP and neovascularization, examined either in the angle using gonioscopy or in retina using ophthalmoscopy, combined with visual field loss or optic nerve head cupping, the diagnose neovascular glaucoma was given.

Retinal detachment: Presence of retinal detachment was determined by ophthalmoscopy and reported without time-to-event.

Vasculopathy: Radiation-induced vasculopathy was found as micro-occlusions and intraretinal microvascular abnormalities adjacent to ischemic areas as seen from ophthalmoscopy.

Anterior complications

Cataract: Lens opacity resulting in gradual deterioration of the visual acuity. It was diagnosed by slit lamp examination or ophthalmoscopy.

Dry eye: Reduced production of lacrimal fluid occurring after irradiation of the lacrimal gland and resulting in itching, redness and general discomfort in the eye. These symptoms formed the basis for the diagnosis while measurements from Schirmer's test were used to confirm diagnosis.

Data analysis

For each endpoint, we pre-specified relevant normal tissues (and their corresponding dose metrics) and clinical factors for analysis; resulting in more than 50 potential variables per endpoint. Pre-specification was performed by a consultant ophthalmologist and a radiation oncologist, both with several years of experience in ocular oncology. See details in the analysis plan in Appendix B.

Due to the large number of potential variables, Lasso (least absolute shrinkage and selection operator) regression analysis was used to perform variable selection among the numerous and correlated variables [10,11]. The variables with the strongest correlation with each outcome were estimated from the regularized method by shrinkage and elimination of variable coefficients. The optimal shrinkage parameter (λ) was determined from 100-fold cross-validation. We used the first standard error of λ to obtain the smallest number of predictors, and thus the simplest model with an acceptable error [12]. We carried out the multivariable regression analyses with the variables selected from the Lasso.

For visual acuity deterioration, we carried out two analyses; one were we included the entire cohort irrespective of pre-treatment visual acuity (group 1, analysis 1); and one in which we examined the visual acuity deterioration for patients with a pre-treatment visual acuity ≤ 0.5 logMAR (but keeping all other analysis details unchanged) (group 1, analysis 2). The risk of visual acuity deterioration was analysed using logistic regression (but including follow-up time as separate variable).

Specific late complications were analysed using Cox's proportional hazards regression [13]. Time was measured from start of radiotherapy to whichever happened first: event, death or loss of follow-up (with patients censored for the two latter). For retinal detachment, time-to-event was missing in the follow-up data, and logistic regression rather than Cox regression was performed (see previous paragraph). Preventive treatments were not made for any of the ocular complications. Treatment was initiated after the complications occurred. As such, the time-to-event was not affected.

Model performance was assessed by Hosmer-Lemeshow for goodness-of-fit of the logistic regression analyses, while concordance index and Brier score were used to evaluate the Cox regression models. Schoenfeld residuals demonstrated no time dependence for any of the variables included, and the proportional hazard assumption was thus assumed not to be violated.

Dose-response for each complication was visualized by plotting the predicted risk of complication/toxicity (at a fixed time point (5 years) for Cox regression) as a function of dose, with all other model variables kept constant. Additionally, the impact of clinical factors, such as tumour height or optic disc-tumour distance, on the risk of toxicity was demonstrated by varying these using relevant clinical values.

The median potential follow-up time was assessed using the inverse Kaplan-Meier estimate [14]. All analyses were performed in RStudio (Version 0.99.467). The full, annotated model fits are available as R files at Electronic Research Data Archive (ERDA) [15].

Results

Patients and descriptive statistics

1020 patients had complete information on clinical characteristics, dose data and visual acuity measures (group 1, analysis 1). 541 patients had pre-treatment visual acuity of ≤ 0.5 logMAR (group 1, analysis 2). 991 patients had complete information on clinical characteristics, dose data and late complications (group 2). Patients could be represented in both groups if they had complete information on all the above variables. See the flowchart in Figure 2 for details on patient data used. The overall median potential follow-up time was 6.1 years (95 % CI 6.0-6.2).

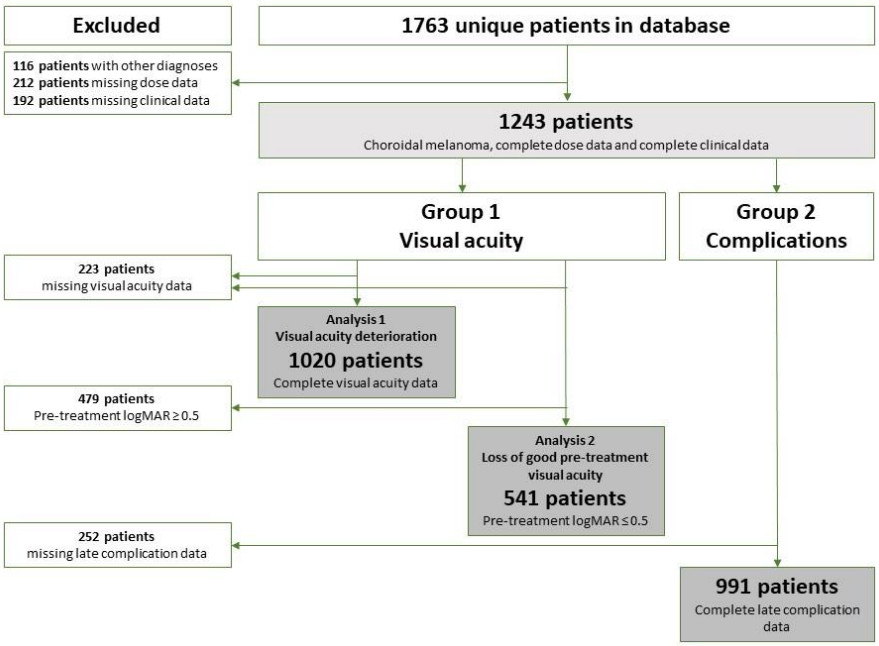

Figure 2: Flowchart describing the used patient data. 1020 patients had complete information on clinical characteristics, dose data and visual acuity measures (group 1, analysis 1). 541 patients had pre-treatment visual acuity of ≤ 0.5 logMAR (group 1, analysis 2). 991 patients had complete information on clinical characteristics, dose data and late complications (group 2). Patients could be represented in both groups if they had complete information on all the above variables.

Patient, tumour and treatment characteristics for both groups are listed in Table 1.

	Group 1 Patients with visual acuity data N=1020	Group 2 Patients with complication data N=991	
Patient and tumour characteristics	**Value (median (IQR))**	**Value (median (IQR))**	
Age (years)	66 (56-75)	65 (55-75)	
Gender male/female	476/544	452/539	
Baseline VA (logMAR)	0.4 (0.2-1.0)	-	
Baseline VA logMAR ≤ 0.5 y/n	541/479	-	
Last VA (logMAR)	1.6 (0.4-2.0)	-	
Last VA logMAR ≤ 0.5 y/n	300/720	-	
Follow-up (years)	5.1 (2.8-8.1)	5.1 (2.9-8.0)	
Largest basal dimension (mm)	11.0 (9.0-13.3)	11.0 (9.0-13.3)	
Height (mm)	4.9 (3.2-7.3)	4.9 (3.2-7.3)	
Optic disc-tumour distance (mm)	4.0 (1.2-7.1)	3.7 (1.1-6.8)	
Macula-tumour distance (mm)	3.0 (0.6-6.8)	3.0 (0.3-6.3)	
Complication		**Number (%)**	**5-year probability of freedom from toxicity (95 % CI)**
Maculopathy		205 (21 %)	79 % (76-82)
Optic neuropathy		135 (14 %)	85 % (82-97)
Neovascular glaucoma		118 (12 %)	87 % (85-89)
Retinal detachment		357 (36 %)	-

Ocular hypertension		66 (7 %)	92 % (90-94)
Vasculopathy		213 (21 %)	76 % (73-79)
Cataract		310 (31 %)	68 % (65-71)
Dry eye		148 (15 %)	84 % (82-87)

Table 1: Descriptive statistics and list of incidences for each complication with 5-year risk of freedom from the complication (based on Kaplan-Meier estimates). The date for retinal detachment was not available, and the actuarial risk was thus not calculated. VA=visual acuity, IQR=interquartile range, logMAR= logarithm of Minimum Angle of Resolution.

Group 1: Visual acuity

Analysis 1 - Visual acuity deterioration

For patients irrespective of initial pre-treatment visual acuity, the risk of visual acuity deterioration correlated with near-maximum macula dose (macula $D_{2\%}$). As did to a smaller extend various other dose metrics (optic disc $D_{2\%}$, retina $D_{20\%}$, globe V_{10Gy} and globe V_{5Gy}) as well as tumour height, optic disc-tumour distance and follow-up time. Odds ratios are listed in Table 2. Figure 3A illustrates the dose-response relationship for macula $D_{2\%}$ for all cases, while Figure 3B illustrates the relationship for three specific tumour heights (3.0, 6.0 and 9.0 mm), respectively.

Analysis 2 – Loss of good pre-treatment visual acuity

For patients with good initial pre-treatment visual acuity, the risk of visual acuity loss correlated with macula $D_{2\%}$ and pre-treatment visual acuity. Additionally, the volume of the optic disc receiving 50% of the prescribed dose (optic disc V_{26Gy}) demonstrated weaker correlation. Besides dose, tumour height and optic disc-tumour distance were the only clinical variables correlated with the risk of loss of pre-treatment visual acuity. Odd ratios are listed in Table 2. Figure 3C and Figure 3D illustrate the dose-response relationship for macula $D_{2\%}$ and for three specific tumour heights.

225 Note the stronger dose-dependence for macula $D_{2\%}$ compared to analysis 1 on all patients
226 irrespective of initial pre-treatment visual acuity.
227
228 Model performance using Hosmer-Lemeshow showed a strong correlation between observed and
229 predicted risk of visual acuity deterioration for both logistic regression models. The model
230 goodness-of-fits are illustrated in Appendix C for both visual acuity analyses.
231

	Analysis 1: Visual acuity deterioration	**Analysis 2: Loss of good pre-treatment visual acuity**
Variables in logistic model	**Odds ratio (95 % CI)**	**Odds ratio (95 % CI)**
Tumour height	1.25 (1.14-1.38)	1.51 (1.29-1.79)
Optic disc-tumour distance	0.98 (0.93-1.03)	0.96 (0.90-1.02)
Optic disc $D_{20\%}$ $^{+}$	-	1.01 (0.58-1.81)
Optic disc $D_{2\%}$ $^{+}$	1.11 (1.01-1.22)	-
Optic disc V_{26Gy} *	-	1.10 (0.90-1.33)
Optic disc V_{5Gy} *	-	1.00 (0.78-1.27)
Macula $D_{2\%}$ $^{+}$	1.18 (1.09-1.28)	1.28 (1.15-1.44)
Retina $D_{20\%}$	1.12 (0.98-1.29)	-
Globe V_{10Gy}	1.11 (0.76-1.61)	1.01 (0.98-1.04)
Globe V_{5Gy}	0.91 (0.63-1.31)	-
Follow-up (1 y increase)	1.08 (1.04-1.13)	-

232 **Table 2:** Odds ratios with 95 % confidence intervals (CI) from multivariable logistic regression
233 analyses. $^{+}$=10 Gy increase, *= 10 %-point increase.

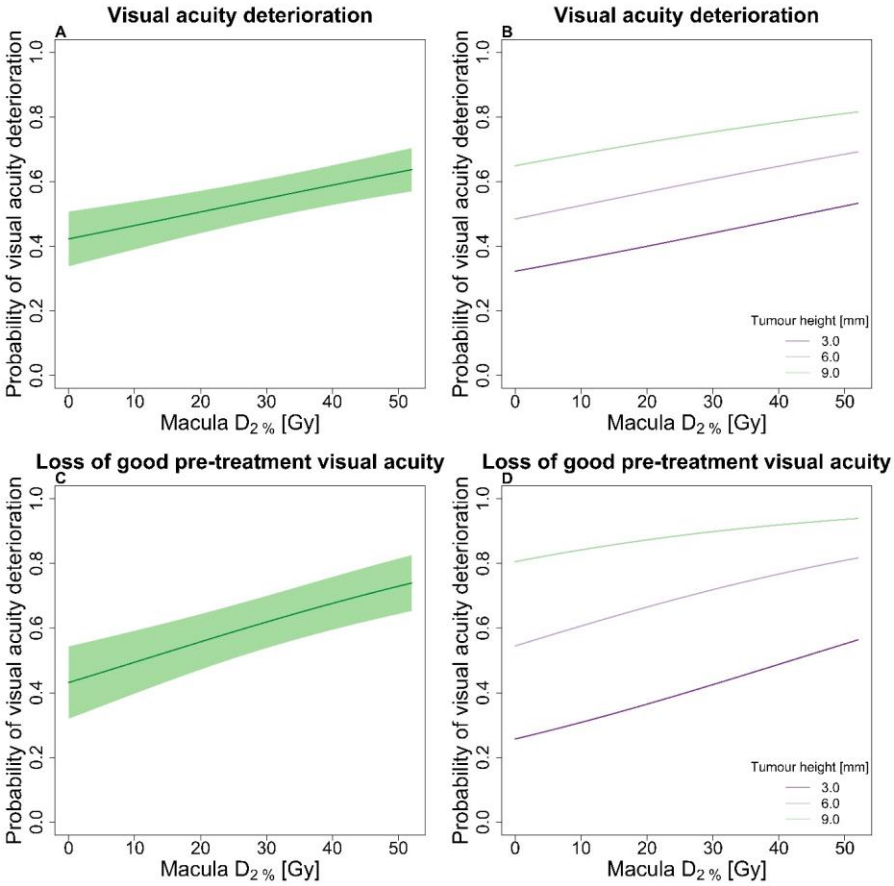

Figure 3: A) Dose response of visual acuity deterioration at 5 years as a function of near-maximum macula dose (macula $D_{2\%}$). The shaded area represents the 95% confidence interval. The model is adjusted for tumour height (4.9 mm), optic disc-tumour distance (4.0 mm), optic disc $D_{2\%}$ (4.0 Gy), retina $D_{20\%}$ (51.7 Gy), globe V_{10Gy} (36% of total eye volume), globe V_{5Gy} (38% of total eye volume) and follow-up (5.1 years). The values were set as the median value for the entire visual acuity group. B) Dose response of visual acuity deterioration at 5 years as a function of macula $D_{2\%}$ for three tumour heights (3.0, 6.0 and 9.0 mm). C) Dose response of pre-treatment visual acuity loss at 5 years after a baseline visual acuity of ≤ 0.5 logMAR as a function of macula $D_{2\%}$. The model is

adjusted for tumour height, optic disc-tumour distance, optic disc V_{26Gy} (0%), optic disc V_{5Gy} (0%), optic disc $D_{20\%}$ (1.3 Gy) and globe V_{10Gy}. D) Dose response of pre-treatment visual acuity loss at 5 years after a baseline visual acuity of ≤ 0.5 logMAR as a function of macula $D_{2\%}$ for the three tumour heights.

Group 2: Complications

The hazard ratios (HRs) including 95% CI for complication data are listed in Table 3. No predictors were found for vasculopathy and no analysis was consequently made for this late complication.

Complication	**Hazard ratio (95 % CI)**
Maculopathy	
Retina $D_{20\%}$ +	1.21 (1.07-1.36)
Optic neuropathy	
Optic disc-tumour distance	0.83 (0.72-0.95)
Optic disc $D_{20\%}$ +	1.15 (0.94-1.41)
Optic disc V_{42Gy} *	1.04 (0.96-1.13)
Neovascular glaucoma	
Tumour height	1.31 (1.16-1.47)
Cornea $D_{20\%}$ +	1.26 (1.12-1.41)
Globe $D_{50\%}$ #	1.00 (0.98-1.02)
Globe V_{52Gy}	0.99 (0.96-1.02)
Optic disc V_{52Gy} *	1.10 (1.05-1.15)
Ocular hypertension	
Tumour height	1.08 (0.96-1.20)

Ciliary body $D_{20\%}$ +	1.46 (1.10-1.95)
Ciliary body V_{26Gy} *	1.10 (0.74-1.64)
Cornea $D_{20\%}$ +	1.06 (0.86-1.30)
Retina $D_{50\%}$	1.01 (0.99-1.03)
Cataract	
Ciliary body V_{26Gy} *	1.31 (1.22-1.40)
Dry eye syndrome	
Optic disc-tumour distance	1.09 (1.05-1.12)
Retinal detachment	**Odds ratio (95 % CI)**
Age at treatment	0.98 (0.97-0.99)
Tumour height	1.15 (1.06-1.25)
Largest base dimension	1.07 (1.00-1.14)
Optic disc-tumour distance	0.88 (0.84-0.91)
Retina V_{52Gy}	1.06 (1.00-1.12)
Retina V_{42Gy}	0.98 (0.93-1.03)

Table 3: Hazard ratios (HR) and 95 % confidence intervals (CI) for each of the complications in multivariable Cox regression analysis. +=10 Gy increase, *=10 %-point increase, # percent of volume relative to eye volume.

Maculopathy

Retina $D_{20\%}$ was the only variable chosen from the Lasso procedure to impact the risk of developing maculopathy, although this relationship was relatively weak. The dose-response for this relationship is illustrated in Figure 4A.

Optic neuropathy

The dose delivered to 20% of the optic disc (optic disc $D_{20\%}$) was the variable with the largest HR for optic neuropathy, but this was also a relatively weak correlation. Figure 4B illustrates the dose-response model for this relationship. Tumour-optic disc distance was the only clinical variable associated with the risk of developing optic neuropathy.

Neovascular glaucoma

The dose delivered to 20% of the cornea (cornea $D_{20\%}$) demonstrated the strongest association with neovascular glaucoma; see illustration in Figure 4C.

Ocular hypertension

Several dose metrics were chosen from the Lasso procedure for ocular hypertension and demonstrated association with the risk of developing this late complication, but ciliary body $D_{20\%}$ was the variable with the strongest correlation (although this was still relatively weak). Figure 4D illustrates this relationship.

Cataract

The volume of the ciliary body receiving 50% of the prescribed dose (ciliary body V_{26Gy}) was the only variable associated with the risk of cataract and this strong relationship is illustrated in Figure 4E.

Retinal detachment

The volume of the retina receiving 100% of the prescribed dose (retina V_{52Gy}) proved to have a considerable impact on the risk of developing retinal detachment after the treatment. Figure 4F illustrates this relationship.

Model performance using concordance index (c-index) and Brier score showed acceptable 5-year accuracy, with the best calibration being for the ocular hypertension and neovascular glaucoma models. The model goodness-of-fits are illustrated in Appendix C for all late complication analyses.

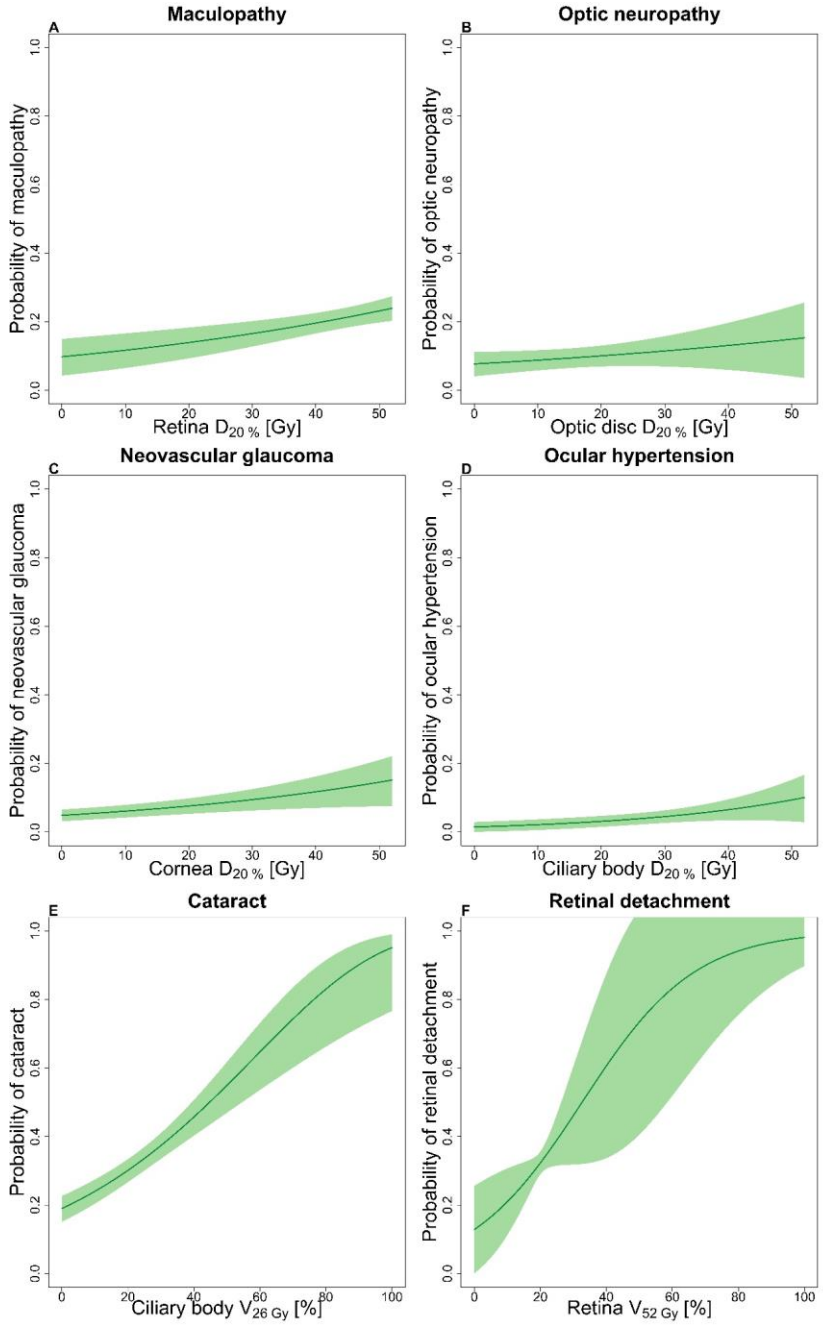
Maculopathy
A
Probability of maculopathy
Retina D20 % [Gy]
Optic neuropathy
B
Probability of optic neuropathy
Optic disc D20 % [Gy]
Neovascular glaucoma
C
Probability of neovascular glaucoma
Cornea D20 % [Gy]
Ocular hypertension
D
Probability of ocular hypertension
Ciliary body D20 % [Gy]
Cataract
E
Probability of cataract
Ciliary body V26 Gy [%]
Retinal detachment
F
Probability of retinal detachment
Retina V52 Gy [%]

285

Figure 4: A) Dose response of maculopathy at 5 years as a function of retina $D_{20\%}$. The shaded area represents the 95% confidence interval of the risk estimate. B) Dose response of optic neuropathy at 5 years as a function of optic disc $D_{20\%}$. The model adjusts for optic disc-tumour distance (3.7 mm) and optic disc V_{42Gy} (0%) and optic disc V_{10Gy} (0%). C) Dose response of neovascular glaucoma at 5 years as a function of cornea $D_{20\%}$. The model adjusts for tumour height (4.9 mm), optic disc V_{52Gy} (0%), globe $D_{50\%}$ (0 Gy) and globe V_{52Gy} (29.1%). D) Dose response of ocular hypertension at 5 years as a function of ciliary body $D_{20\%}$. The model adjusts for tumour height, cornea $D_{20\%}$ (0 Gy), retina $D_{50\%}$ (0 Gy) and ciliary body V_{26Gy} (20%). E) Dose response of cataract at 5 years as a function of ciliary body V_{26Gy}. F) Dose response of retinal detachment at 5 years as a function of retina V_{52Gy}. The model adjusts for retina V_{42Gy}, age at treatment (65 years), tumour height, largest base dimension (11 mm) and optic disc-tumour.

Discussion

In this retrospective study of a large single-institution cohort, we examined relationships between dose delivered to healthy tissue and the occurrence of visual acuity deterioration and late radiation-induced complications after proton therapy for choroidal melanoma. The novelty of this study is the use of advanced statistics to identify risk factors with the strongest impact on each endpoint in multivariable analysis. This was done to robustly explore the full scope of potential dose and volume dependence. Normal tissue dose was important for visual acuity deterioration, and dose to healthy structures was a considerable factor associated with the risk of developing most of the late complications.

Broad, composite endpoints showed correlation with a relatively wide range of normal tissue doses, corresponding to a complex underlying pathophysiology. As such, dose metrics for several normal structures appeared to have an impact on visual acuity deterioration. The maximum dose to the

macula, $D_{2\%}$, was, however, associated with the largest effect. In the group with good pre-treatment visual acuity, where a change was more likely to be caused by the treatment, rather than other factors, we also found the steepest dose-response relationship (Figure 3C). Interestingly, tumour height was directly associated with risk of visual acuity deterioration and the correlation was stronger than the maximum dose to the macula. This confirms similar findings reported previously, where tumour height was the most important factor for visual loss and risk of enucleation [16–18].

Specific complication endpoints were to a larger extend related to dose metrics from specific healthy structures, potentially representing a more direct link between structures, pathophysiology of radiation damage, and the resulting clinical complications.

Remarkably, radiation dose had little importance on the risk of optic neuropathy (Table 3) even though the Lasso analysis selected multiple closely correlated optic disc dose metrics. This was reflected in the developed dose-response models for optic neuropathy, which had poor prognostic value as the model contained no obvious threshold. Our data indicated that the most important predictor for the risk of developing optic neuropathy was the proximity of the tumour to the optic disc.

For maculopathy, we found no effect of radiation to the macula – in contrast to Gragoudas et al., where macular exposure to radiation was main risk factor [19]; this study was, however, based on a selected group of patients and the prescribed tumour dose was higher than in our study (70 CGE vs ~57 CGE) [18]. We found that dose delivered to 20% of the retina (retina $D_{20\%}$) was the only variable with impact on the risk of maculopathy. We speculated that retina $D_{20\%}$ potentially represented a surrogate for tumour extension or for macula $D_{2\%}$ and consequently for visual acuity deterioration.

Post-treatment retinal detachment was not defined as a risk factor but as an endpoint in our analysis, because retinal detachment involving the macula can cause visual impairment. It was the most frequent side-effect in this cohort. Egger et al. found that only 29.3% of patients experienced no retinal detachment [20]. However, the rate essentially depends on how it is diagnosed. We speculate that some of the retinal detachments included in our data might have been present already before the treatment was initiated even if the retina normalised after the treatment. It could not be determined whether the retinal detachments were caused by tumour decay or direct radiation damage. We did find that tumour height, posterior located tumours, and volume of the retina receiving full prescription dose (retina V_{52Gy}) increased the risk.

Dose metrics for several normal tissue structures were identified from the Lasso analysis to increase the risk of ocular hypertension. Dose to 20% of the ciliary body (ciliary body $D_{20\%}$) was found to have the strongest impact; possibly an indirect effect from radiation-induced damage of the trabecular meshwork preventing drainage of produced aqueous [21].

In addition to ocular hypertension, neovascular glaucoma involve new vessel formation in the anterior segment, indicating a component of ischemia and release of angiogenic factors. Therefore, neovascular glaucoma is a more complex endpoint that is likely to be caused from multiple various factors, but it remains unknown which specific variables are main risk factors. We found that tumour height was the variable with the strongest impact on the risk of neovascular glaucoma, while the dose delivered to 20% of the cornea surface (cornea $D_{20\%}$) and the volume of the optic disc receiving maximum dose (optic disc S/V_{52Gy}) increased the risk. This is in line with previous findings by Mishra et al. that also reported increased tumour height, dose to anterior critical structures (lens or ciliary body), and dose to the optic disc as main risk factors [22]. Daftari et al. advocated sparing of radiation to the anterior segment to prevent neovascular glaucoma [23]. Sparing of dose to the anterior structures during treatment is, however, difficult since tumour

coverage and sparing of the macula and the optic disc are prioritized. This could explain why the Lasso analysis selects globe $D_{50\%}$ and globe V_{52Gy} as risk factors (Table 3).

Cataract was a common side-effect in our cohort; occurring in one third of patients. The lens has been reported to be the most radiosensitive ocular structure [24]. However, we found the volume of ciliary body that received 50% of the dose (ciliary body V_{26Gy}) as the most important variable for the development of cataract, most likely since development of cataract is a multifactorial event with various risk factors. Additionally, we speculate that the finding of ciliary body dose might reflect an indirect effect of the dose to the lens. To explore this further, we performed an explorative analysis including solely the lens DVH along with clinical factors. We found that the maximum dose to the lens (lens $D_{2\%}$) was important for the risk of cataract when no other dose metrics were included in the selection process (results not shown). This has been reported in previous studies [25,26]. Phacoemulsification can, however, be carried out safely even after proton therapy, and visual acuity can be recovered after surgery.

For dry eye syndrome, the only variable associated with increased risk was the optic disc-tumour distance; the longer the distance the higher the risk. This lack of dependence could possibly be explained by the lack of lachrymal gland contouring in the treatment planning system; consequently, it was not possible to explore all relevant dose relationships [27].

We used advanced statistical methodology for selecting appropriate variables to include in the analyses. In this way, we included the predictors associated with risk of each specific endpoint, while excluding variables with no clear impact. The use of Lasso for variable selection is a well-established and robust method to handle many variables. It is, however, recognised that the method has problems when the included variables are highly correlated. Additionally, the cross-validation performed to select the optimal shrinkage parameter has previously been described to select too

many non-informative variables. This may explain the selection of competing dose metrics for some of the toxicities in this study [28].

It is important to recognize that this was a retrospective analysis. It is a considerable strength of the study, however, that complications were recorded during follow-up and extracted from the database for the purpose of this study. Unfortunately, the time-to-event information for visual acuity deterioration and retinal detachment were not available. We did, however, include total follow-up time in the model to adjust for any time-effect. Furthermore, the effect of tumour volume was not explored. Since tumours often have complex shapes (e.g. mushroom shape) the volumes are difficult to measure, making tumour height a much more precise measure. Additionally, tumour height has been the standard variable to include in analyses in the literature. As such, the knowledge gained from including tumour height in the model is valuable and can be comparable to the literature.

We report relatively low prevalence of some of the radiation-induced toxicities compared to previous works [29], which might be a result of using a personalized treatment plan and a dedicated eyeline for all treatments. However, another reason for the low prevalence could be that mild toxicities were underreported. Toxicity reporting is most likely heterogeneous among centres; indicating lack of standardization in terms of diagnosing radiation-induced ocular toxicities. Finger et al. have established guidelines for the diagnosis of retinopathy but an expansion to the remaining complications are needed [30].

Limited data currently exist on the tolerance of various eye structures to radiation dose for external beam photon treatment. It has solely been described by the QUANTEC review for the optic nerve and the chiasm [31]. The maximum dose (D_{max}) to the optic nerve was related to the risk of late radiation-induced optic neuropathy, with maximum tolerable dose for normo-fractionated (1.8-2

Gy/fraction) external beam photon treatment at around 60 Gy. Importantly, these data cannot be compared directly to the hypo-fractionated physical doses used for choroidal melanomas. Similarly, the current results will not be applicable to brachytherapy (Ru-106) [32] due to different dose-fractionation/dose-rate effects and different underlying radiobiology of the radiation modalities.

The dose-response models established in this study can ultimately help guide the radiation oncologists' decisions on optimal treatment and gaze direction during the treatment planning. The established models could additionally guide future treatment planning to maintain a low level of radiation-induced toxicities. Individualized toxicity risk estimates may also help treatment modality selection – keeping in mind that besides filter and margins, there are no further optimization options during proton planning in most currently available treatment planning systems. Further dedicated studies are needed for each treatment modality, especially if individualised treatment modality selection and optimisation is to be realised.

References

[1] Finger PT. Radiation therapy for choroidal melanoma. Surv Ophthalmol 1997;42:215–32.

[2] Groenewald C, Konstantinidis L, Damato B. Effects of radiotherapy on uveal melanomas and adjacent tissues. Eye (Lond) 2013;27:163–71.

[3] Thariat J, Grange JD, Mosci C, et al. Visual Outcomes of Parapapillary Uveal Melanomas Following Proton Beam Therapy. Int J Radiat Oncol Biol Phys 2016;95:328–35.

[4] Chauvel P, Mandrillon P, Brassart N, et al. Status report on the installation of proton and neurontherapy in centre Antoine-Lacassagne 1815:1815–7.

[5] Mandrillon P, Farley F, Brassart N, et al. Commissioning and implementation of the MEDICYC cyclotron programme. Proc. 15th Int. Conf. Cyclotrons their Appl. Caen, Fr., 1989.

[6] Cambria R, Hérault J, Brassart N, et al. Proton beam dosimetry: a comparison between the Faraday cup and an ionization chamber. Phys Med Biol 1997;42:1185–96.

[7] Courdi A, Caujolle JP, Grange JD, et al. Results of proton therapy of uveal melanomas treated in Nice. Int J Radiat Oncol Biol Phys 1999;45:5–11.

[8] Elliott DB. The good (logMAR), the bad (Snellen) and the ugly (BCVA, number of letters read) of visual acuity measurement. Ophthalmic Physiol Opt 2016;36:355–8.

[9] Lim LA, Frost NA, Powell RJ, et al. Comparison of the ETDRS logMAR, compact reduced logMar and Snellen charts in routine clinical practice. Eye 2010;24:673–7.

[10] Ternès N, Rotolo F, Michiels S. Empirical extensions of the lasso penalty to reduce the false discovery rate in high-dimensional Cox regression models. Stat Med 2016;35:2561–73.

[11] Efron B, Hastie T. Computer age statistical inference: Algorithms, evidence, and data science. 2016.

[12] Hastie Trevor and Qian Junyang. Glmnet Vignette 2014:1–42.

[13] Cox DR. Regression models and life-tables. J R Stat Soc Ser B 1972;34:187–220.

[14] Schemper M, Smith TL. A note on quantifying follow-up in studies of failure time. Control Clin Trials 1996;17:343–6.

[15] Espensen CA, Kiilgaard JF, Appelt AL, et al. Descriptive document for analyses in manuscript (DOI for linked data will be available at the time of publication). ERDA 2020.

[16] Seddon JM, Gragoudas ES, Egan KM, et al. Uveal melanomas near the optic disc or fovea. Visual results after proton beam irradiation. Ophthalmology 1987;94:354–61.

[17] Egan KM, Gragoudas ES, Seddon JM, et al. The Risk of Enucleation after Proton Beam Irradiation of Uveal Melanoma. Ophthalmology 1989;96:1377–83.

[18] Thariat J, Grange J, Mosci C, et al. Visual Outcomes of Parapapillary Uveal Melanomas Following Proton Beam Therapy 2016;95:328–35.

[19] Gragoudas ES, Li W, Lane AM, et al. Risk factors for radiation maculopathy and papillopathy after intraocular irradiation☆. Ophthalmology 1999;106:1571–8.

[20] Egger E, Schalenbourg A, Zografos L, et al. Maximizing local tumor control and survival after proton beam radiotherapy of uveal melanoma. Int J Radiat Oncol 2001;51:138–47.

[21] Moses RA. Adler's Physiology of the eye. 5th ed. 1970.

[22] Mishra KK, Daftari IK, Weinberg V, et al. Risk Factors for Neovascular Glaucoma After Proton Beam Therapy of Uveal Melanoma: A Detailed Analysis of Tumor and Dose–Volume Parameters. Int J Radiat Oncol 2013;87:330–6.

[23] Daftari IK, Char DH, Verhey LJ, et al. Anterior segment sparing to reduce charged particle radiotherapy complications in uveal melanoma. Int J Radiat Oncol Biol Phys 1997;39:997–1010.

[24] Seibel I, Cordini D, Hager A, et al. Cataract development in patients treated with proton beam therapy for uveal melanoma. Graefe's Arch Clin Exp Ophthalmol 2016;254:1625–30.

[25] Thariat J, Jacob S, Caujolle JP, et al. Cataract avoidance with proton therapy in ocular melanomas. Investig Ophthalmol Vis Sci 2017;58:5378–86.

[26] Mathis T, Rosier L, Meniai F, et al. The Lens Opacities Classification System III Grading in Irradiated Uveal Melanomas to Characterize Proton Therapy-Induced Cataracts. Am J Ophthalmol 2019;201:63–71.

[27] Thariat J, Maschi C, Lanteri S, et al. Dry Eye Syndrome After Proton Therapy of Ocular Melanomas. Int J Radiat Oncol Biol Phys 2017;98:142–51.

[28] He K, Wang Y, Zhou X, et al. An improved variable selection procedure for adaptive Lasso in high-dimensional survival analysis. Lifetime Data Anal 2018.

[29] Dendale R, Lumbroso-Le Rouic L, Noel G, et al. Proton beam radiotherapy for uveal melanoma: Results of Curie Institut-Orsay Proton Therapy Center (ICPO). Int J Radiat Oncol Biol Phys 2006;65:780–7.

[30] Finger P, Kurli M. Laser photocoagulation for radiation retinopathy after ophthalmic plaque radiation therapy. Br J Ophthalmol 2005;89:730–8.

[31] Mayo C, Martel MK, Marks LB, et al. Radiation Dose-Volume Effects of Optic Nerves and Chiasm. Int J Radiat Oncol Biol Phys 2010;76:28–35.

[32] Espensen CA, Appelt AL, Fog LS, et al. Predicting visual acuity deterioration and radiation-induced toxicities after brachytherapy for choroidal melanomas. Cancers (Basel) 2019.

Formatted: English (United States)